11-2008

Viability of Travel-time Sensitivity Testing for Estimating Uncertainty of Tomographic Velocity Models: A Case Study

Matthew G. Averill

Kate C. Miller

Vladik Kreinovich
The University of Texas at El Paso, vladik@utep.edu

Aaron A. Velasco
The University of Texas at El Paso, aavelasco@utep.edu

Comments:
Technical Report: UTEP-CS-08-40

Viability of Travel-time Sensitivity Testing for Estimating Uncertainty of Tomographic Velocity Models: A Case Study

Journal:	*Geophysics*
Manuscript ID:	GEO-2008-0386
Manuscript Type:	Case History
Date Submitted by the Author:	15-Nov-2008
Complete List of Authors:	Miller, Kate; University of Texas at El Paso, Dept. of Geological Sciences, Averill, Matthew; Anadarko Petroleum Co. Kreinovich, Vladik; University of Texas at El Paso, Computer Science Velasco, Aaron; University of Texas at El Paso, Geological Sciences
Keywords:	tomography, refraction, resolution
Area of Expertise:	Seismic Inversion, Seismic Velocity/Statics

Viability of Travel-time Sensitivity Testing for Estimating Uncertainty of Tomographic Velocity Models: A Case Study

Matthew G. Averill[*], Kate C. Miller *(corresponding author)*, Vladik Krenovich[**], and Aaron A. Velasco
Department of Geological Sciences, University of Texas at El Paso, El Paso, TX 79968, Email: miller@geo.utep.edu

[*]*Present Address: Anadarko Petroleum Co., 1201 Lake Robbins Dr., P.O. Box 1330, Houston, TX 77251-1330, Email: Matthew.Averill@anadarko.com*
[**] *Department of Computer Science, University of Texas at El Paso, El Paso, TX 79968*

Submitted to Geophysics

November 14, 2008

ABSTRACT

Seismic tomography is now a common approach to estimating velocity structure of the Earth, regardless of whether the data sources are earthquake recordings or controlled sources such as explosions, airguns or Vibroseis. Seismic tomography is convenient to implement because it requires little to no *a priori* knowledge of Earth structure and is much less time consuming than forward modeling schemes. Despite it's convenience, the method still lacks satisfactory quantitative assessments of model reliability. Here we explore the viability of applying travel-time sensitivity testing that uses a modified Cauchy distribution as its statistical foundation to assessing the uncertainty in velocity models produced with seismic tomography. Using a crustal refraction survey as a test data set, we find that this approach produces a more realistic estimate of the velocity uncertainty than does either a resampling approach or travel-time sensitivity testing that uses a Gaussian distribution as its statistical foundation. The

velocity uncertainty estimates provide an important complement to other estimates of model reliability including checkerboard tests.

INTRODUCTION

A variety of methodologies exist for developing velocity models of the Earth at different scales from seismic travel time data, including both forward modeling and inverse approaches (*e. g.* Zelt and Smith, 1992; Iyer and Hirahara, 1993; Zelt and Barton, 1998). Among these, seismic tomography has become increasingly common, in part because it is convenient and easy to implement and in part because models obtained through tomography are commonly considered to be more objective than those developed through forward modeling schemes that are subject to the interpretational bias of the analyst.

A long-standing difficulty with all methods for developing velocity models of the Earth, including seismic tomography, is the lack of satisfactory quantitative assessments of model reliability. Here we consider two measures of model reliability: spatial resolution and uncertainty, where spatial resolution is a measure of the ability of the model to distinguish between two adjacent features, and uncertainty is a measure of the degree to which a model parameter is actually known. In assessing a seismic tomography result, the analyst typically uses a combination of overall misfit of observed and calculated travel times for the final model, a plot of ray coverage and checkerboard tests to obtain a qualitative assessment of overall reliability (Zelt and Barton, 1998; Parsons et al., 1999). For example, an analyst would consider areas of the model in which ray coverage is high and reproduction of checker geometry good, to be very reliable.

Whereas, estimates of travel time uncertainty are commonly made, estimates of model uncertainty are rare.

In inverse methods in which the model is parameterized in terms of layers and velocity gradients (e.g. Lutter et al., 1990; Zelt and Smith, 1992), the diagonal elements of the resolution matrix and the square root of the diagonal elements of the model covariance matrix give a quantitative sense for the number of rays that sample a model parameter and the standard error or uncertainty for each model parameter. These assessments are typically only used in a relative sense because they do not account for a number of other sources of error in the modeling process (e.g. Zelt and Smith, 1992). Clearly, forward modeling approaches offer essentially no error assessments, other than the analyst's intuition.

Here we explore the use of travel-time sensitivity testing that uses a modified Cauchy distribution as its statistical foundation as a method for assessing the uncertainty in velocity models produced with seismic tomography. An advantage of this methodology over qualitative assessments of ray coverage maps and checkerboard tests, alone, is that it produces an uncertainty estimate in velocity units for each cell in the model. We show that another advantage of this approach is that it produces a more realistic assessment of model uncertainty than sensitivity testing that assumes a Gaussian distribution of travel time error. We also find that the Cauchy approach gave a more realistic estimate of uncertainty than a jack-knife approach.

We take a case study approach by applying seismic tomography and reliability estimation to a data set from a crustal refraction survey from southern New Mexico, USA, known as the Potrillo Volcanic Field (PVF) seismic experiment (Averill, 2007).

The survey design is typical of modern wide-angle reflection/refraction surveys that seek to image the crust and upper mantle. Nevertheless, our results are applicable to a wide-range of tomographic studies from near-surface imaging projects to those that seek to image the whole Earth.

SEISMIC TOMOGRAPHY

Seismic tomography determines the velocity structure of the earth through inversion of body-wave travel-time data (e.g., Iyer and Hirahara, 1993). Seismic energy can be generated either by an earthquake or a "controlled" source (e.g. explosion, air-gun, Vibroseis source) for earth structure Arrival times for the body waves are determined from recording of the source energy at seismographs strategically located within a study area. The model is typically defined in terms of boxes or pixels with constant slowness (the inverse of velocity) distributed in two or three dimensions. A variety of algorithms exist for implementing the tomography. Here, we use a non-linear 3-D tomographic inversion algorithm that can produce a relatively high-resolution model, as well as reproduce large velocity contrasts (Hole, 1992).

The algorithm linearizes the non-linear relationship between seismic travel time and slowness by inverting for small perturbations to a reference slowness model. As a result, iterations are required to achieve a final slowness model (Hole, 1992). Each iteration involves a forward travel time calculation, an inversion for changes to the slowness model, and updating and smoothing of a new slowness model. Travel times from each source to each receiver in a slowness model are calculated using a finite difference method based on the eikonal equation (Vidale, 1988). Typically, the initial model is a simple 1-D model derived from an initial fit to the cloud of observed travel

times and/or existing knowledge of regional geology and seismic velocity. Subsequent travel time calculations use updates to the slowness field as a starting model.

In the next step, the inversion is accomplished with a back projection method that uses the difference between observed and calculated travel times (the travel time residuals) to solve for changes to the slowness model (Hole, 1992). The model is then updated with the slowness changes and smoothed with a moving average filter before input to the next iteration. This filter helps stabilize the inversion and assure that the linearization assumptions in the algorithm are valid by decreasing the magnitude of slowness perturbations and spreading them over a wider area in the updated model (Hole, 1992).

To obtain a final model, it is typical to run 4 to 7 iterations for each of a series of progressively smaller moving average filters or smoothers. This series, known as the smoothing schedule, maintains stability while still allowing progressively shorter wavelength features to develop in the model (Zelt and Barton, 1998). According to standard statistical procedure (e. g. Papoulis, 1984), we consider a model to be acceptable when the root-mean square (RMS) travel time residual reaches a value roughly equal to the error in picking travel times in the data. For our example of crustal data this is usually 0.1 s.

SEISMIC SURVEY AND VELOCITY MODEL

The seismic survey was comprised of 8 explosive shots with an average spacing of 35 km that were recorded by 793 seismic seismographs deployed at variable spacing between 100 and 600 m along a 205 km transect (Figure 1; see Averill (2007) for a complete description). Shots varied in size between 500 and 1000 kg. Record sections

for two of the shot points (Figure 2) show that first arrivals are visible across the entire transect except where disrupted by cultural noise in the urban El Paso portion of the profile. A total of 4633 first arrival times were picked from the data and assigned uncertainties using an automated scheme based on an empirical relationship between a signal-to-noise ratio estimate calculated within a window of 250 ms on either side of the pick and a travel time uncertainty (Zelt and Forsyth, 1994).

For the example shown here, a 1D model that included strong velocity gradients at approximately 2 and 35 km depth below the surface was provided to the inversion as the initial reference model (Figure 3). Whereas, a number of other starting models yielded similar final models, this initial model helped preserve strong velocity gradients associated with interfaces at depths determined by modeling of reflected phases in the data (Averill, 2007).

Even though the survey was nearly two-dimensional, the tomography was carried out in three dimensions using a 230 x 25 x 68 grid of blocks with dimensions of 1 km on a side in order to avoid inducing errors by projecting shot and station locations on to a line. For simplicity, all results are displayed in two-dimensions. On all figures that display velocity, values were determined from a weighted average of the model values in the Y (north-south) direction, where the weight was determined from the ray coverage in the cell. Thus cells with more ray coverage contribute proportionally more to the displayed value. 2D displays of ray coverage represent a sum of the hit count in the y-direction for a given depth z and distance, x.

The inversion was carried out with a smoothing schedule of 6 moving average filters with 6 iterations for each filter dimension (Table 1). The dimensions of the

smoothing filter was gradually reduced in order to improve model resolution and reduce the RMS travel time misfit while still maintaining the stability of the inversion process. The final model (Figure 3) had an RMS travel time misfit of 0.08 s.

Overall, the final model is characterized by strong velocity heterogeneity in the upper five kilometers of the crust that gives way to less heterogeneity with depth. The velocity structure of the upper 5 km clearly reflects surface structure where features with velocities of ca. 4.6 and 5.2 km/s correspond to mountain ranges and features with velocities ca. 2.0 to 4.4 km/s correspond to known middle to late Tertiary basins in the study area. Between ca. -3 km and -12 km depth are longer wavelength changes in velocity with values of 5.7 to 6. 4 km/s. These may correspond to geologic structures that developed during Mesozoic to early Tertiary time across the region (Averill and Miller, submitted; Averill, 2007). Below 15 km, a step up in the 6.5 km/s contour from ca. 20 km to 15 km suggests a lateral change in crustal composition in the mid-crust. Ray coverage bottoms out in the upper mantle where velocities reach 7.9 km/s. The model shows that the thickness of the crust is ca. 30-35 km in the region. Further details of the geologic and tectonic interpretation of the model can be found in Averill and Miller (submitted) and Averill (2007).

COMMONLY USED ASSESSMENTS OF MODEL RELIABLITY

Here we examine what the most commonly used assessments of model reliability, including travel time misfits, ray coverage, checkboard, and jack-knife tests, tell us about the reliability of the Potrillo Volcanic Field velocity model. We then compare these to the results of sensitivity testing.

Travel Time Misfit

Both the overall RMS travel-time misfit as well as a graph that shows individual travel-time misfits for each shot receiver pair are commonly used as a guide in evaluating model reliability. For the final PVF model overall RMS misfit was very low at 0.08 s. For crustal refraction surveys, an overall RMS misfit of 0.1s is generally considered to be excellent. Detailed examination of the travel time fits (Figure 4) shows that individual misfits are locally 0.2 s or higher for a number of regions in the model. For this model, large misfits (> 0.2 s) are associated with arrivals that have ray paths that pass through low velocity shallow basins. These misfits are the result from the algorithm's inability to fit the large lateral velocity gradients associated with the basins given the sparse shot coverage and 1 km cell size used in the tomography. Given these specific observations of misfits, an interpreter would conclude that in general, the model over-estimates the velocities within the basin (ie. the calculated travel time is generally early compared to the observed travel time within basins). Another area with consistently high misfit values occur between model coordinates 175 and 200 km. These can be attributed to greater uncertainty in the first arrival time picks due to the low signal to noise ratio in the data associated with cultural noise in the El Paso metropolitan area.

Ray Coverage

Ray coverage diagrams are also tools for qualitatively assessing model reliability. Unlike in medical tomography, results from seismic tomography are usually characterized by heterogeneous and anisotropic ray coverage. That is the value of ray coverage may vary greatly from block to block in the model and the variety of angles at which rays enter and exit a block is often very limited. An interpreter would normally

consider regions with high ray coverage, as more reliable than those with lower ray coverage. However, this assumption must be take with care as a significant portion of the ray coverage in models developed from active source seismic data comes from regions where rays are travelling almost entirely in the horizontal plane. By contrast, the algorithm produces the most reliable results when the angles at which rays enter and exit a cell are highly varied.

These types of concerns are quite evident in the ray coverage for the final PVF model (Figure 3B). Coverage is most highly concentrated above -7 to -8 km. The angles at which rays pass through any given block are also more varied in this region because the velocity gradient is high so rays turn rapidly over shorter distances. Nevertheless, there are a few regions of high coverage where ray direction is dominantly horizontal. Rays are most highly concentrated in the region between shotpoints 3 and 5 because the receiver spacing is 100 m there. Outside this area, receiver spacing is 2 to 6 times greater.

At greater depth, the ray coverage is more heterogeneous. At these depths, velocity gradients are gentle, resulting in longer ray paths that turn more slowly. The diagram does show that ray paths concentrate at ca. 15 km and at ca. 35 km, which are local zones with relatively high velocity gradients. The gradient near 15 km depth is calculated by the tomography whereas, the one at 35 km is probably still influenced by the gradient placed there by the initial 1D model based on constraints from wide-angle reflections (Figure 2). The ray angles in these high gradient regions are strongly biased toward the horizontal, which may suggest somewhat lower model reliability to an interpreter despite the high coverage values.

Checkerboard Testing

Checkerboard testing is commonly used as a qualitative assessment of both velocity uncertainty and structural reliability in tomographic velocity models. Checkerboard testing typically involves using the seismic survey geometry to calculate synthetic travel times for a velocity model that is comprised of a simple background model to which a checkerboard-like perturbation has been added. The synthetic travel times are then used as the input data to the same iterative inversion scheme used to generate the final velocity model. The background model used in the synthetic travel time calculation is used as the starting model in the test. Typically, some sort of pseudo-checkerboard pattern such as a two-dimensional sinusoid with an amplitude and wavelength appropriate to the scale of features of interest is used (Zelt, 1998).

The results of the test are evaluated on the extent to which the inversion scheme is able to reconstruct the original checkerboard pattern in various regions of the model. To assess resolution, an analyst would consider the extent to which both the shape and amplitude of the original checker was recovered. The semblance value or "resolvability" between the exact and recovered checkerboard anomalies has also been used as a more quantitative approach to assessing resolution (Zelt and Barton, 1998).

In our work, we implemented a checkerboard testing procedure similar to those in common use in seismic tomography studies. (e.g., Hearn and Ni, 1994; Zelt and Forsyth, 1994; Vasco and Johnson, 1998). Our procedure began by adding a 5% sinusoidal velocity perturbation to a background model derived by averaging our final velocity model at each depth interval to obtain a 1D model. We calculated synthetic travel time using our seismic survey geometry for two perturbed models, one with perturbations with wavelengths of 10x5 km in the horizontal and vertical directions, respectively, and one

with perturbations with wavelengths of 20 x10 km (Figure 5). These wavelengths were chosen to be larger than the final smoothing operator of 4x2x2 km used in the inversion and to be comparable to the size of features we hoped to resolve in the modeling process.

We then followed the same inversion scheme used to develop the final model, including the 1D background model and the synthetic travel times calculated from the perturbed models as inputs. The results (Figure 6), show the extent to which the sinsusoidal pattern of Figure 5 was recovered. Results for the 10x5 km checkerboard test (Figure 6a) show good recovery of the sinsusoidal pattern in terms of both shape and amplitude for the uppermost row of checkers. In the next row, between 5 and 10 km depth, is some recovery of the shape of the anomalies and amplitude recovery reaches a maximum of 1.5% compared to the original 5% anomaly. Below 10 km, virtually none of the velocity perturbations are recovered. Results were similar for the test using 20x10 km sinusoids (Figure 6b) except that it showed some recovery of checkers to depths of 18 to 20 km in the western half of the model.

A fundamental shortcoming of checkerboard testing is clearly evident in the models that show checker recovery. That is that even though velocity perturbations are not recovered in the lower half to two-thirds of the model, it would not be appropriate to interpret the result as showing that the tomography gives us no information about velocity there. For example, we know that the calculated travel times from the final model fit the observed travel times at large offset well (Figure 4), so the deeper parts of the model are likely to give us at least some useful information. In the end, the checkerboard test really only gives information on whether perturbations of a particular wavelength can be resolved given the survey geometry.

There are a variety of strategies for varying the checkerboard test such as testing models with perturbations at several more wavelengths, shifting or rotating the pattern by changing the phase of the sine function, and changing the amplitude of the velocity perturbation (e.g., Zelt, 1999). However, none of these are likely to change the fact that the survey geometry simply may not recover perturbations in the deeper part of the model. Changes in amplitude are particularly tricky as smaller amplitudes can be hard to recover and larger amplitudes cause steep velocity gradients in the model that tend to affect the stability of the inversion. Furthermore, checkerboard testing does not take into account other sources of error such as the inherent uncertainty in picking arrival times in the data.

Jack-knife Approach

Resampling techniques, of which jackknifing is one, have sometimes been used to estimate velocity uncertainty for tomography (e. g. Lees and Crosson, 1989). This class of statistical methods may be useful for geophysical data sets because it is insensitive to the statistical properties of the data (Tichelaar and Ruff, 1989).

For the PVF data, we conducted a preliminary test of a jackknife approach. This method involves dividing the data into N sets by omitting a $1/N$ portion of the data and then uses the subset of the data as input to the modeling process (e.g., Good, 2005). In our test, we divided our travel time data set in two (i.e., N=2) approximately equal subsets defined by the odd and even station numbers. Two velocity models were then calculated on the basis of the subsets using the same procedure described in the section entitled “Seismic Survey and Velocity Model”. To visualize the effects of omitting half the data from the tomography, the RMS difference between the final model and each of

those computed from the subsets was computed, and the RMS differences were then averaged.

These results (Figure 7) provide information on the model that is explained by the portion of the data that was removed. The plot shows that lateral variability in the RMS velocity differences are observed. For example values of the RMS difference are relatively high in the central and deeper parts of the model space and near the surface at shot point 1. This suggests that these parts of the model are probably most affected by decimation of the data. A shortcoming of this approach appears to be that the overall RMS velocity differences were generally low, below 0.040 km/s, which is significantly less than an experienced analyst would expect for the velocity uncertainty. For this reason, we moved on to look at the viability of travel-time sensitivity testing.

TRAVEL TIME SENSITIVITY TESTING

In travel-time sensitivity testing a Monte Carlo approach is used to examine the effect of uncertainty or error in the travel-times picks on uncertainty in the velocity model. We initially assumed that the picking error for the travel times had a Gaussian distribution. When the results of this approach turned out to be underestimating uncertainty, we turned to a different statistical method, which only makes assumptions about the upper bounds of measurement errors, and thus allows for all possible probability distributions within these bounds.

Sensitivity Testing Using A Gaussian Distribution

Building on traditional techniques for processing uncertainty in science and engineering, we initially assumed that the picking errors for the travel times are independent and normally distributed with zero mean and known standard deviation (e. g.

Rabinovich, 2005). Testing then proceeds by adding random travel time perturbations with a Gaussian distribution to the observed travel times and using these new travel times as input to an inversion process that includes the same steps used to generate the final velocity model. The sequence of travel-time perturbation followed by inversion is repeated *N* times, e.g. 14 times in this case. The RMS difference in velocity between the final model and each of the models produced in the sensitivity test is then computed. The velocity uncertainty is an average of the *N* RMS differences.

For the PVF data, we calculated 14 different velocity models from travel time data sets that were generated by adding random time perturbations with a Gaussian distribution that had a standard deviation of 0.15 s. We used the same inversion steps that produced the final model to produce each of these velocity models. The RMS velocity difference plot obtained from this effort (Figure 8) is characterized by large areas with values of less than 0.015 km/s and a few isolated areas with values of 0.1 to 0.15 km/s. Even smaller average uncertainty values are obtained when the random time perturbations are calculated using Gaussian distributions with standard deviations equal to the empirical uncertainty determined for each individual travel time (described in section on the seismic survey and velocity model).

From experience with working with these kinds of data sets, we recognized that uncertainty values of 0.015 km/s for velocity were likely to be unrealistically small from a physical perspective. An explanation for these small values is that our assumption of error independence is probably not appropriate for active-source travel-time data, because the very process of picking involves correlation. For example, an analyst typically makes travel time picks on a traces with higher signal-to-noise ratios on the basis of arrivals on

adjacent traces with lower signal-to-noise-ratios. These conditions violate the assumption of data having errors that are uncorrelated.

Sensitivity Testing Using Interval Techniques

An alternative approach, that takes possible bias and correlation in the measurements into account is to use interval techniques (e.g., Trejo et al., 2001; Kreinovich and Ferson, 2004). In this approach, we assume that we know only the upper bounds Δ_i on the measurement errors, and thus we can allow for all possible probability distributions within these bounds. For the case of developing a velocity model, it might be desirable to estimate the upper bound Δ on the approximation error of the result of the data processing (ie. the tomography). An efficient way for computing Δ is based on a mathematical trick: if we simulate measurement errors as independent and as having a Cauchy distribution with parameter Δ_i, then the result of data processing is Cauchy distributed with the desired parameter Δ (e.g. Papoulis, 1984; Spiegel, 1992). This is a mathematical trick and not a real assumption about the measurement errors, since we know that the errors are located on an interval, whereas the Cauchy distribution itself goes beyond this interval. This process produces the worst-case error for the data processing results (Trejo et al., 2001; Kreinovich and Ferson, 2004), i.e. in our cat the velocity model.

We applied the interval technique to travel-time sensitivity testing of the PVF data set using the same procedure described earlier, except that we added random perturbations with a Cauchy distribution to the travel time data rather than using a Gaussian distribution. To generate perturbations with a Cauchy distribution, we took the tangent of a set of random numbers uniformly distributed between $\pi/2$ and $\pi/2$ to produce

a Cauchy distribution with values between -∞ and ∞. We then scaled these values to produce a set of perturbations with a Cauchy parameter of 0.15 s, the upper bound on the travel time uncertainty. Again, we used our tomography procedure to calculate 14 different velocity models from travel time data sets generated through this process. These results were used to calculate the model uncertainty using the maximum likelihood method (Trejo et al., 2001; Kreinovich and Ferson, 2004).

The initial results (Figure 9a) again gave an uncertainty pattern that make sense in a qualitative way, but that was physically meaningless. For example the uncertainty values correspond reasonably well with the density and geometry of ray coverage in the model (Figure 3). The lowest uncertainty values are in the upper part of the model and along paths of greatest ray coverage. The highest values or regions of highest uncertainty are at depths of 30 to 35 km, and near the center of the model, where ray coverage is low. Another high value area lies beneath El Paso (between shot points 5 and 6), where ray coverage is low compared to the shallow crust in the rest of the model due to urban noise which decreased both the number and quality of travel times that could be identified.

With a range of 15 to 20,820 km/s, the result was still not useful for quantitative estimates of velocity uncertainty. We interpret the large values as resulting from worst-case combinations of original measurement error resulting in huge error estimates. For example, the process of generating random perturbations with a Cauchy distribution may have produced numerous perturbations of ±0.15 s for adjacent arrivals at short offsets, which would normally have had very low travel time uncertainties. The tomography runs individually could then have produced wildly different velocity values for a given cell,

resulting in extraordinarily high uncertainty values. In practice, it is clear that such combinations are likely to be rare and are certainly physically meaningless.

In an attempt to produce physically reasonable uncertainty values, we weighted the random travel-time perturbations using Cauchy distributions with scale parameters set to the empirically-determined uncertainty for the arrival which ranged between 0.02 s and 0.15 s for the data. At first, this seemed like a reasonable way to dampen the influence of worst-case travel time error estimates with a physically meaningful value, the "known" travel time uncertainty. Qualitatively, this approach produced a very similar pattern to that seen in the first attempt. But again, the velocity uncertainty estimates, while lower at 0 to 865 km/s, were still physically meaningless.

In a second attempt to produce physically reasonable uncertainty values, we decided to look for error bounds that are valid within a given certainty, rather than for the worst-case error bounds. In practice, this meant restricting ourselves to bounds guaranteed with a certain confidence, e.g., bounds that are guaranteed with a confidence of 95%, and then dismissing the upper 5% of the perturbations. To find such bounds, we "cut-off" the upper and lower 5% of the Cauchy distribution. To do this, we found the threshold value (x_0) for which the probability of exceeding this value is 5% (or any other desired cut-off probability p_0), and then replace values x for which $x \geq x_0$ with x_0 and for $x \leq -x_0$ with $-x_0$. For the Cauchy distribution, we have determined that a 95% confidence interval is obtained for bounds of $-12.71 \leq x_0 \leq 12.71$ (Appendix A). We then applied these cutoffs to the perturbations, and proceeded with sensitivity testing as described earlier.

The results show a pattern of model uncertainty similar to those obtained previously, but with physically reasonable values (Figure 9b). Velocity uncertainties range from approximately 0.01 to 0.30 km/s. The lowest values are found near the shot points, and along paths of highest ray coverage (Figure 3b). The highest uncertainty values lie near the center of the model below 10 km depth and beneath the urban El Paso region between shot points 5 and 6. In the center of the model, low ray coverage is probably the primary control on the high uncertainty values. Beneath El Paso, not only is ray coverage lower, but travel time uncertainties are high due to the low signal-to-noise ratio of the data there. Thus both probably contribute to high uncertainty values there. Calculations using a 90% confidence level resulted in a similar pattern, but with a lower average uncertainty and a range of 0.005 to 0.230 km/s.

DISCUSSION

The primary goals of a geologic interpretation of a velocity model are typically to determine the geometry of subsurface structure and the type of rock and/or fluid that is present at depth. The credibility of the geologic interpretation rests in large part on knowledge of model reliability. To date, the common practice of applying checkerboard tests to models derived from seismic tomography has been very helpful in providing guidance to the interpreter on the size of geologic features that might be distinguishable in different regions of a model for a given experiment geometry. However, this methodology has little to offer efforts to assess the error in the velocity estimate at any given point in the model.

In principle travel-time sensitivity testing that assume a Gaussian distribution of the travel time error and jack-knife approaches have the potential to provide information

on the uncertainty. Indeed, this case study shows that in a relative sense, the pattern of uncertainty produced by these methods can be useful in determining where the model is more or less reliable. Nevertheless, they provide unreasonably low estimates of model uncertainty in an absolute sense. It is perhaps for this reason, that workers rarely include uncertainty estimates in their assessments of velocity models derived from tomography. By contrast, our results show that incorporation of modified interval techniques into travel time sensitivity testing does produce reasonable estimates of velocity uncertainty.

Our work also illustrates two reasons why it might be important to routinely include estimates of velocity uncertainty along with checkerboard tests in assessments of model reliability. First, because the sensitivity testing depends on the effects of errors in the travel times, it provides completely different information from checkerboard testing, which depends more strongly on survey geometry. An example of the importance of this difference is clearly evident in the upper 10 km of the model between shot points 5 and 6, where on the basis of the checkerboard test alone, an analyst would interpret the model as being highly reliable because the checkers are well reproduced (Figure 6). By contrast, the result from the travel time sensitivity testing (Figure 9B) shows this region as having some of the highest velocity uncertainty in the entire model. This result is consistent with high values of travel time uncertainty that were empirically-determined for arrivals in this region and that were caused by the high levels of cultural noise in the city of El Paso, Texas. Without, actually performing the sensitivity testing, an analyst would not have been able to evaluate exactly how the high travel time uncertainty actually affected the velocity estimate.

A second reason for carrying out the sensitivity testing is to obtain at least some information on the reliability of the velocity model below 10 to 15 km in depth, where the checkerboard test (Figure 6) resolves virtually no structure. In this same region, the result from sensitivity testing (Figure 9b) shows considerable heterogeneity in the uncertainty values that could be used in the interpretation of the model.

CONCLUSIONS

Using a case study approach, this work both introduces a new method for estimating uncertainty in velocity models produced from seismic tomography and examines the strengths and weaknesses of current methods for estimating model reliability. We demonstrate that with a statistical model appropriate to the data, in this case one provided by interval techniques, it is possible to routinely produce geophysically reasonable estimates of model uncertainty based on the data uncertainty. As in our study, earlier work, (e. g. Doser et al., 1998) has demonstrated that travel time sensitivity testing based on a Gaussian distribution of the travel time error is a possible approach to estimating model uncertainty, but that the results included uncertainty values that were too small to be useful in an absolute sense, even though the patterns produced were clearly useful in a relative sense.

The travel time sensitivity testing is an important complement to checkerboard testing in assessing reliability because it can show how data error propagates into model error. By contrast, the more common practice of checkerboard testing gives information on how the survey geometry and the tomography algorithm affect the resolution of features in the subsurface. Many survey geometries result in poor resolution in parts of the model. By routinely neglecting to calculate estimates of model uncertainty, workers

have been missing the opportunity to gain at least some knowledge of model reliability in those parts of the model that are not well resolved in checkerboard tests.

The ultimate goal of calculating a velocity model is often to gain some knowledge of the lithology and/or fluid content of regions of the subsurface. The fact that the physical properties of subsurface materials often display overlap with one another already poses a considerable challenge to efforts to find a one to one correspondence between velocity and lithology and/or fluid. Knowledge of the uncertainty in the velocity estimates provided by sensitivity testing is essential to assessing the reliability of lithologic interpretation of velocity models.

Acknowledgments: This project was supported by Texas Advanced Research Program grant 003661-0019-2001 and NSF grants EAR-0207794, EAR-0225670, and HRD-0734825. Additional funding was provided to Averill by a GK-12 fellowship from NSF grant DGE-0538623 and a Dodson Fellowship from the University of Texas at El Paso. The instruments used in the field program were provided by the PASSCAL facility of the Incorporated Research Institutions for Seismology (IRIS) through the PASSCAL Instrument Center at New Mexico Tech. Data collected during this experiment is a available through the IRIS Data Management Center. The facilities of the IRIS Consortium are supported by the National Science Foundation under Cooperative Agreement EAR-0552316 and by the Department of Energy National Nuclear Security Administration. We especially thank Steven Harder, Galen Kaip, and Carlos Montana for technical support, and the many volunteers from UTEP and elsewhere, who invested their time and energy to prepare and deploy the instruments.

APPENDIX A

The standard Cauchy distribution is characterized by the probability function:

$$f(x) = \frac{1}{\pi}\frac{1}{1+x^2}.$$

We are given a small probability (e.g., $p_0 = 5\%$), and we want to find the value x_0 such that the probability that $|x| \geq x_0$ is exactly p_0. In other words, we want the probability that $x \geq x_0$ or $x \leq -x_0$ to be equal to p_0. Since the Cauchy distribution is symmetric, the probability that $x \leq -x_0$ is equal to the probability that $x \geq x_0$. Therefore, the probability $(prob)$ that $|x| \geq x_0$ is equal to twice the probability that $x \geq x_0$:

$$p_0 = prob(|x| \geq x_0) = 2 \bullet prob(x \geq x_0).$$

It is known that for the Cauchy distribution, the corresponding cumulative distribution function has the form:

$$F(x_0) = prob(x \leq x_0) = \frac{1}{\pi}\int_{-\infty}^{x_0}\frac{dx}{1+x^2},$$

$$F(x_0) = \frac{1}{\pi}(\arctan(x_0) - (-\frac{\pi}{2})) = \frac{1}{\pi}\arctan(x_0) + \frac{1}{2}.$$

Thus,

$$prob(x \geq x_0) = 1 - prob(x \leq x_0),$$

$$prob(x \geq x_0) = 1 - \frac{1}{\pi}\arctan(x_0) - \frac{1}{2},$$

$$prob(x \geq x_0) = \frac{1}{2} - \frac{1}{\pi}\arctan(x_0).$$

Therefore,

$$p_0 = 2 \bullet prob(x \geq x_0) = 1 - \frac{2}{\pi}\arctan(x_0).$$

So, we have

$$\frac{2}{\pi}\arctan(x_0) = 1 - p_0,$$

hence

$$\arctan(x_0) = \frac{\pi}{2}(1 - p_0),$$

and finally,

$$x_0 = \tan(\frac{\pi}{2}(1 - p_0)).$$

If we want confidence level $1 - p_0$, we must solve for the cut-off value x_0. In particular, for a confidence level of 95% (i.e. p_0= 0.05) we must use the value:

$$x_0 = \tan(\frac{\pi}{2} \bullet 0.95) \approx 12.706.$$

Vice-versa, if we use the cut-off value (x_0), we get the bounds, which are valid with confidence level $1 - p_0$, where

$$p_0 = 1 - \frac{2}{\pi}\arctan(x_0).$$

When p_0 is small, we can get simpler approximate expressions for x_0 and p_0. Namely, by definition of a tangent,

$$x_0 = \tan(\frac{\pi}{2} - \frac{\pi}{2}p_0) = \frac{\sin(\frac{\pi}{2} - \frac{\pi}{2}p_0)}{\cos(\frac{\pi}{2} - \frac{\pi}{2}p_0)}.$$

In turn, we know that $\sin(\frac{\pi}{2} - \alpha) = \cos(\alpha)$ and $\cos(\frac{\pi}{2} - \alpha) = \sin(\alpha)$, so

$$x_0 = \frac{\cos(\frac{\pi}{2} p_0)}{\sin(\frac{\pi}{2} p_0)},$$

and for small θ, $\sin\theta \approx \theta$ and $\cos\theta \approx 1$, therefore

$$x_0 \approx \frac{1}{\frac{\pi}{2} p_0} = \frac{2}{\pi p_0},$$

and

$$p_0 \approx \frac{2}{\pi x_0}.$$

REFERENCES

Averill, M. G., 2007, A lithospheric investigation of the southern Rio Grande Rift: Ph.D. Dissertation, University of Texas at El Paso.

Averill, M. G., and K. C. Miller, submitted, Upper crustal structure of the southern Rio Grande Rift: Implications for Mesozoic to Recent structural evolution, *in* Hudson, M. R. and T. Grau, eds., New Perspectives on the Rio Grande Rift: From Tectonics to Groundwater: Geological Society of America Special Paper.

Doser, D.I., K. D. Crain, M. R. Baker, V. Kreinovich, and M. C. Gerstenberger, 1998, Estimating uncertainties for geophysical tomography: Reliable Computing, **4**, 241-268.

Good, P. I., 2005, Resampling Methods: A Practical Guide to Data Analysis, Birkhäuser, 218 pp.

Hearn, T.M., and J. F. Ni, 1994, Pn velocities beneath continental collision zones: the Turkish-Iranian Plateau: Geophysical Journal International, **117**, 273-283.

Hole, J.A., 1992, Nonlinear high-resolution three-dimensional seismic travel time tomography: Journal of Geophysical Research, **97**, 6553-6562.

Iyer, H. M., and K. Hirahara, eds., 1993, Seismic Tomography: Theory and Practice, Chapman and Hall, London, 842 pp.

Kreinovich, V., and S.Ferson, 2004, A new Cauchy-based black-box technique for uncertainty in risk analysis: Reliability Engineering and Systems Safety, **85**, 267-279.

Lees, J. M. and R. S. Crosson, 1989, Tomographic inversion for three-dimensional velocity structure at Mount St. Helens using earthquake data: Journal of Geophysical Research, **94**, 5,716-5,728.

Lutter, W.J., R.L. Nowack, , and L.W. Braile, 1990, Seismic imaging of upper crustal structure using travel times from the PASSCAL Ouachita Experiment, Journal of Geophysical Research, **95**, 4621-5631.

Papoulis, A., 1984, Probability, Random Variables, and Stochastic Processes, 2nd edition: McGraw-Hill.

Parsons, T., R. E. Wells, M. A. Fisher, E. Flueh, U. S. ten Brink, 1999, Three-dimensional velocity structure of Siltezia and other accreted terranes in the Cascadia forearc of Washington: Journal of Geophysical Research, **104**, 18,015-18,039.

Rabinovich, S., 2005, Measurement Errors and Uncertainties: Theory and Practice: Springer-Verlag.

Sheskin, D., 2004, Handbook of Parametric and Nonparametric Statistical Procedures: Chapman & Hall/CRC.

Spiegel, M. R. 1992, Theory and Problems of Probability and Statistics: McGraw-Hill.

Tichelaar, B. W. and L. J. Ruff, 1989, How good are our best models?: Jackknifing, bootstrapping and earthquake depth: EOS, Transactions of the American Geophysical Union: **70**, 593, 605-606.

Trejo, R., and V. Kreinovich, 2001, Error Estimations for indirect measurements: Randomized vs. deterministic algorithms for `black-box' programs, in

Rajasekaran, S., P. Pardalos, J. Reif, and J. Rolim, eds., Handbook on Randomized Computing: 673-729.

Vasco, D.W., and L.R. Johnson, 1998, Whole earth structure estimated from seismic arrival times: Journal of Geophysical Research, **103**, 2,633-2,671.

Vidale, J.E., 1988, Finite-difference calculation of travel-times: Bulletin of the Seismological Society of America, **78**, 2,062-2,076.

Zelt, C. A., 1998. Lateral velocity resolution from three-dimensional seismic refraction data: Geophysical Journal International, **135**, 1,101-1,112.

Zelt, C. A., and R.B. Smith, 1992, Seismic travel time inversion for 2-D crustal velocity structure: Geophysical Journal International, **108**, 16-34.

Zelt, C. A., and D. A. Forsyth, 1994. Modeling wide-angle seismic data for crustal structure Grenville province: Journal of Geophysical Research, **99**, 11,687-11,704.

Zelt, C. A., and P. J. Barton, 1998. 3D seismic refraction tomography: A comparison of two methods applied to data from the Faeroe Basin: Journal of Geophysical Research, **103**, 7,187-7,210.

TABLES

Table 1. Smoothing Schedule for Final Velocity Model

Smoother Dimensions (X x Y x Z cells)	No. Iterations	Starting RMS Misfit (s)	Final RMS Misfit (s)
96 x 24 x 24	6	0.29	0.24
48 x 24 x 16	6	0.24	0.21
24 x 12 x 8	6	0.21	0.16
12 x 8 x 6	6	0.16	0.12
6 x 4 x 2	6	0.12	0.09
4 x 2 x 2	6	0.08	0.07

FIGURE CAPTIONS

Fig. 1. Topographic map showing the location of the Potrillo Volcanic Field (PVF) seismic survey. Stars are shot point locations. Small blue dots are receiver locations. Black box outlines map view of model space used in the tomography.

Fig. 2. Seismic records from shot points 1 and 6 showing data quality and approximate trend of travel times input to the tomography.

Fig. 3 Results of the tomography. A.) The final velocity model gridded at a 1 km interval. Region of significant ray coverage is highlighted with illumination. Inset shows graph of 1D velocity model used as an initial input to the tomography. B.) Plot of ray coverage for final model.

Fig. 4. Graph of observed travel times (gray) input to the tomography and calculated travel-times obtained from the final velocity model. Travel-time residuals (observed – calculated) are plotted as light gray dots at the bottom of the graph.

Fig. 5. Sinusoidal velocity perturbations used in checkerboard tests. A.) The 10x5 km sinusoidal checkerboard; B.) The 20x10 km sinusoidal checkerboard.

Fig. 6. Velocity perturbations recovered in each checkerboard test. A.) Checkers recovered from 10x5 km perturbations. B.) Checkers recovered from 20x10 km perturbations.

Fig. 7. Average RMS difference between the final velocity model and those produced from decimated travel time data in the jackknife test.

Fig. 8. Average RMS difference between the final velocity model and those produced through travel time sensitivity testing using a Gaussian distribution of random perturbations to the travel-time data.

Fig. 9. Average RMS difference between the final velocity model and those produced through travel time sensitivity testing using Cauchy distributions to produce the random perturbations to the travel-time data. A. Average RMS difference produced using a Cauchy distribution for the perturbations. B. Average RMS difference produced with a modified Cauchy distribution. Perturbation values were limited to a 95% confidence interval.

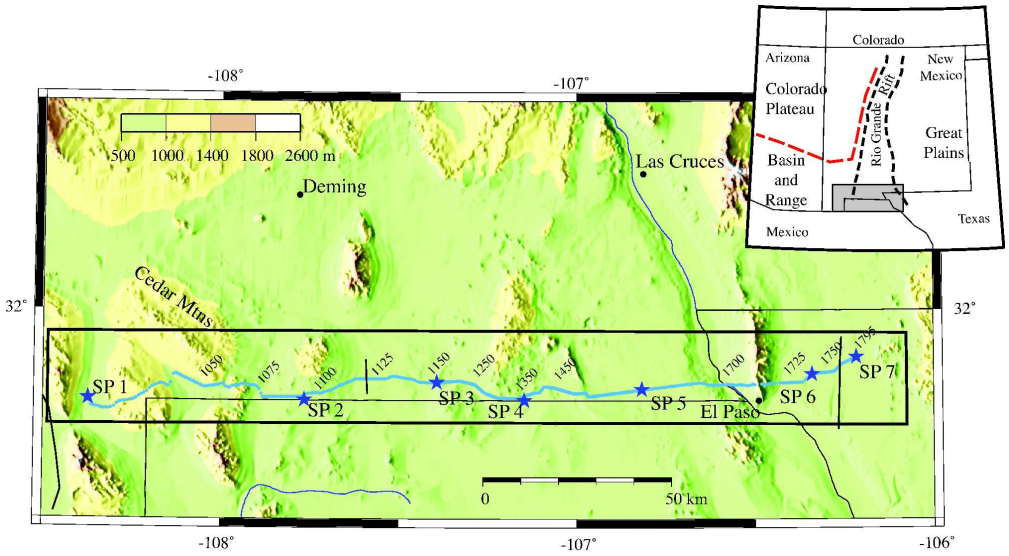

Figure 1 (Averill et al)

Fig. 1. Topographic map showing the location of the Potrillo Volcanic Field (PVF) seismic survey. Stars are shot point locations. Small blue dots are receiver locations. Black box outlines map view of model space used in the tomography.
255x179mm (600 x 600 DPI)

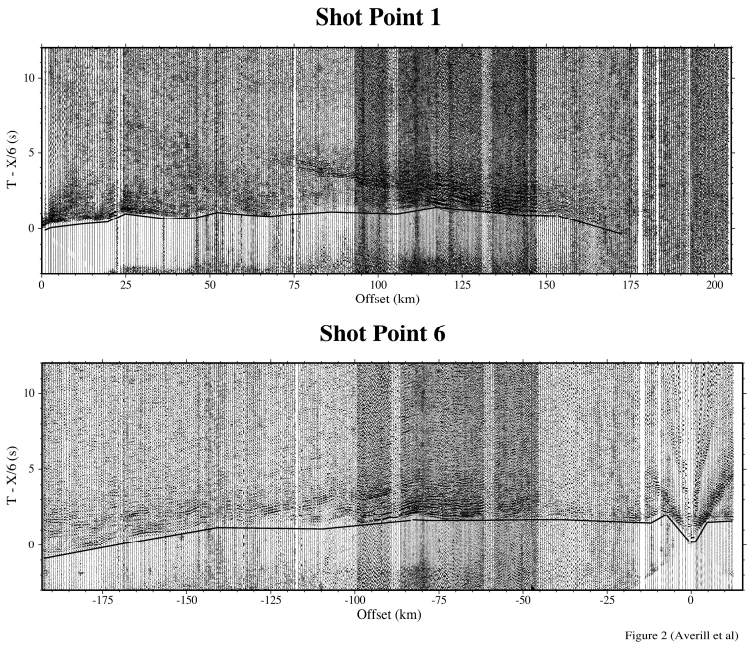

Fig. 2. Seismic records from shot points 1 and 6 showing data quality and approximate trend of travel times input to the tomography.
307x196mm (600 x 600 DPI)

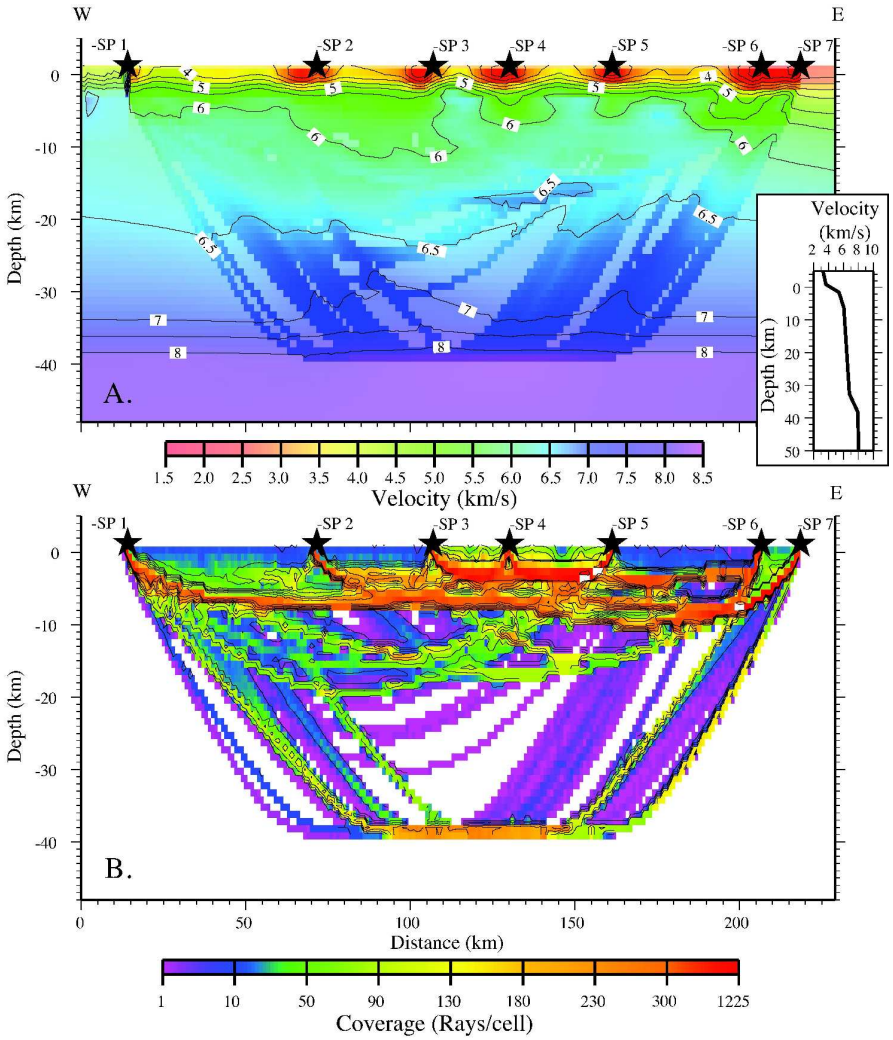

Figure 3 (Averill et al.)

Fig. 3 Results of the tomography. A.) The final velocity model gridded at a 1 km interval. Region of significant ray coverage is highlighted with illumination. Inset shows graph of 1D velocity model used as an initial input to the tomography. B.) Plot of ray coverage for final model.
212x238mm (600 x 600 DPI)

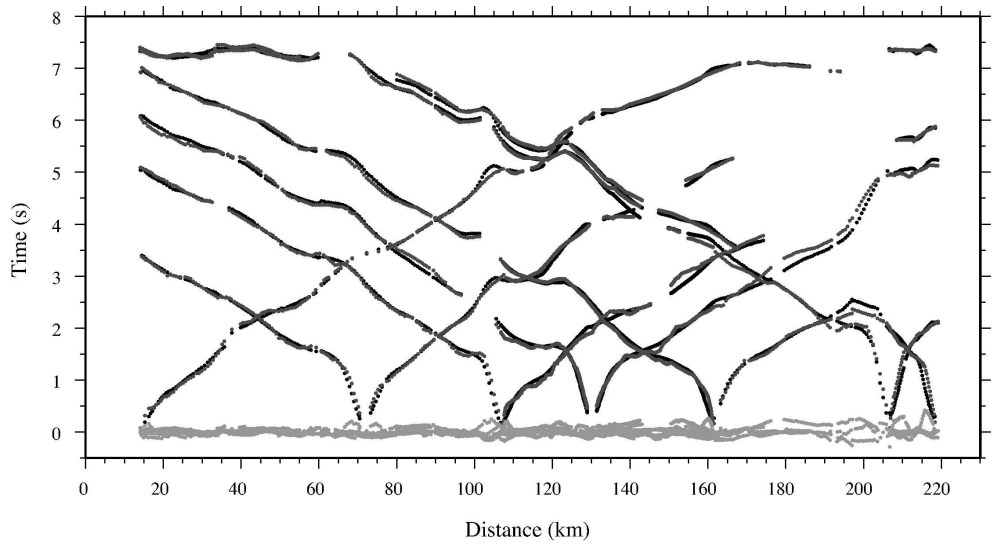

Figure 4 (Averill et al)

Fig. 4. Graph of observed travel times (gray) input to the tomography and calculated travel-times obtained from the final velocity model. Travel-time residuals (observed □ calculated) are plotted as light gray dots at the bottom of the graph.
192x178mm (600 x 600 DPI)

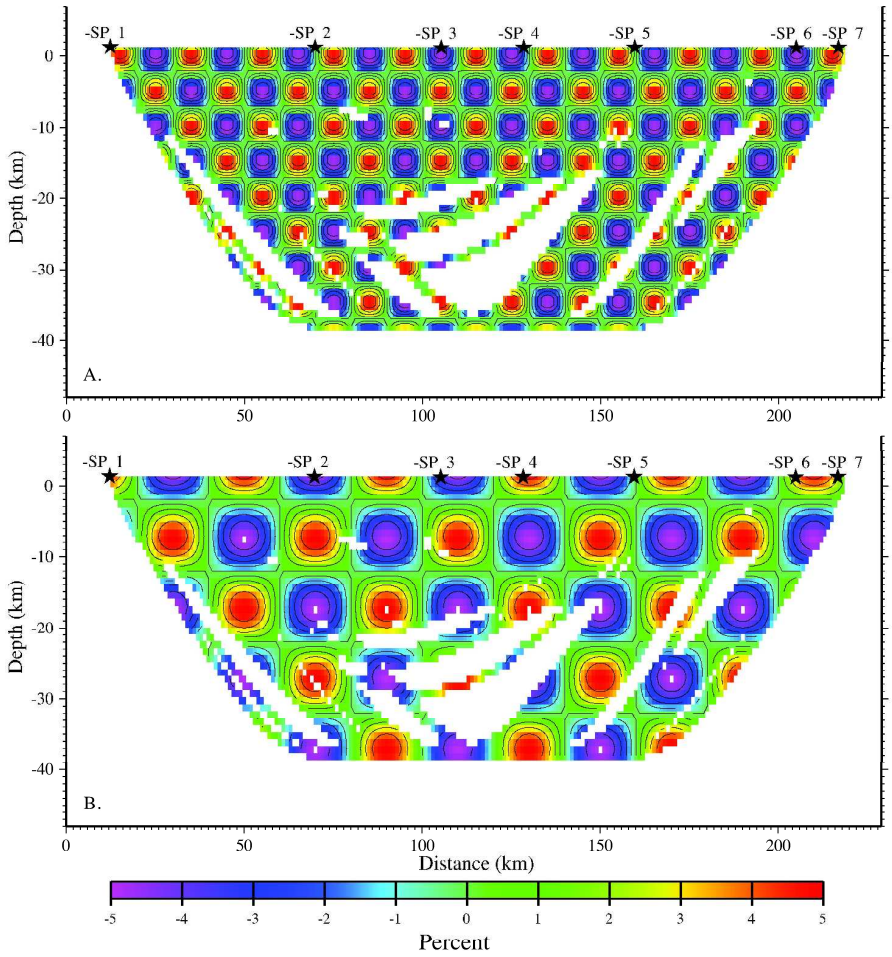

Figure 5 (Averill et al)

Fig. 5. Sinusoidal velocity perturbations used in checkerboard tests. A.) The 10x5 km sinusoidal checkerboard; B.) The 20x10 km sinusoidal checkerboard.
194x250mm (600 x 600 DPI)

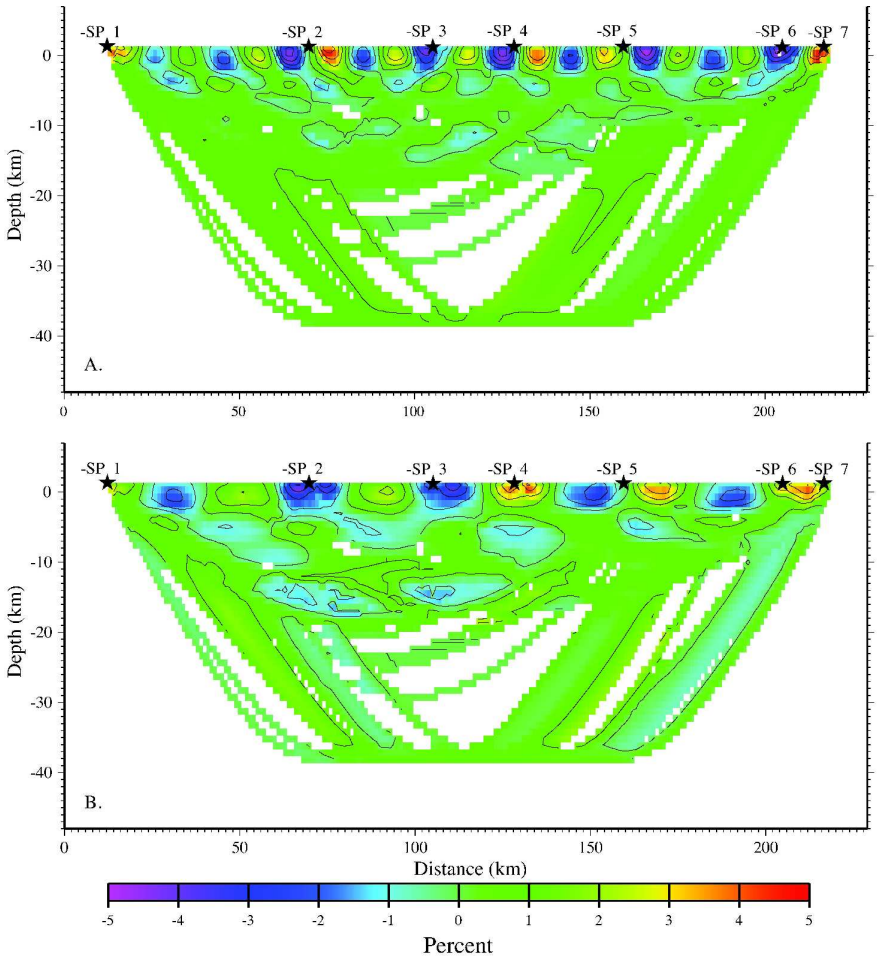

Figure 6 (Averill et al)

Fig. 6. Velocity perturbations recovered in each checkerboard test. A.) Checkers recovered from 10x5 km perturbations. B.) Checkers recovered from 20x10 km perturbations.
186x254mm (600 x 600 DPI)

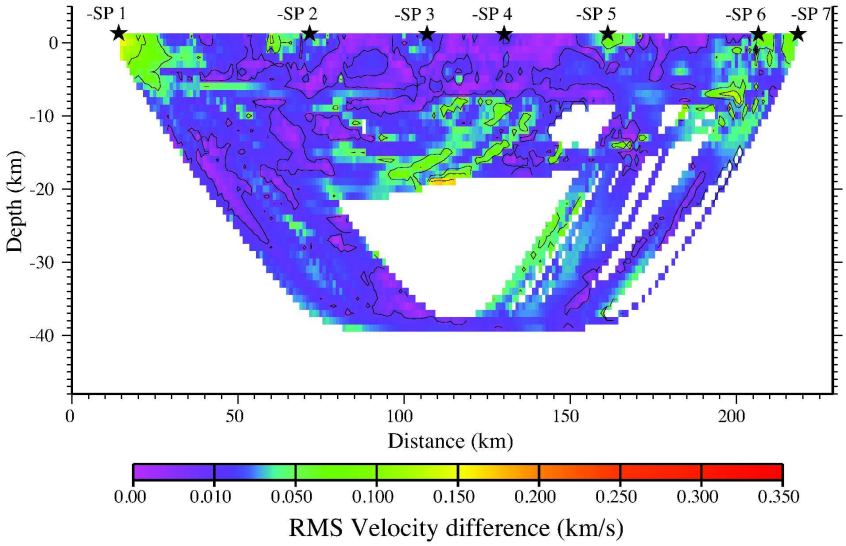

Figure 7 (Averill et al)

Fig. 7. Average RMS difference between the final velocity model and those produced from decimated travel time data in the jackknife test.
172x229mm (600 x 600 DPI)

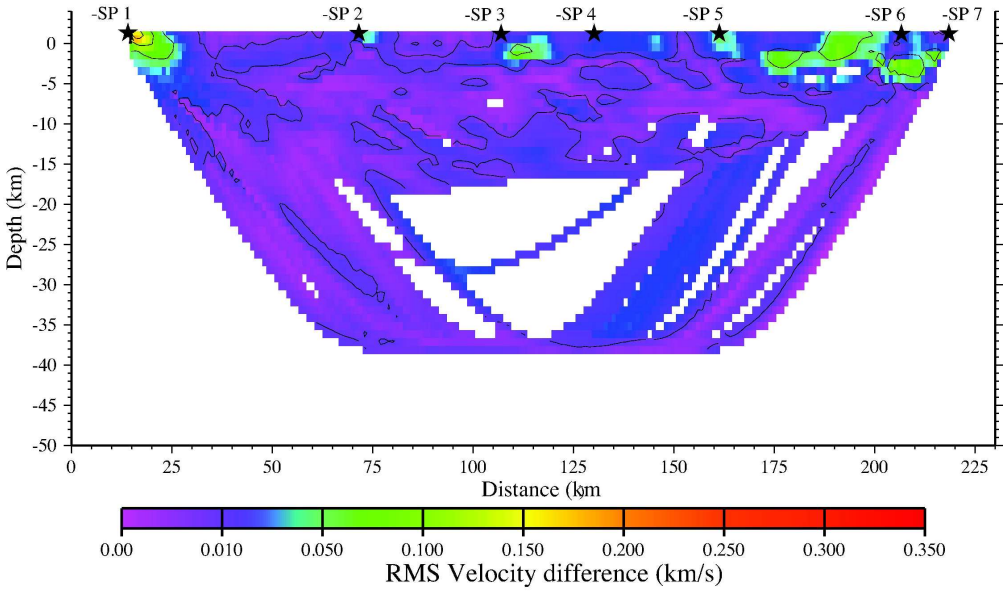

Figure 8 (Averill et al)

Fig. 8. Average RMS difference between the final velocity model and those produced through travel time sensitivity testing using a Gaussian distribution of random perturbations to the travel-time data.
189x225mm (600 x 600 DPI)

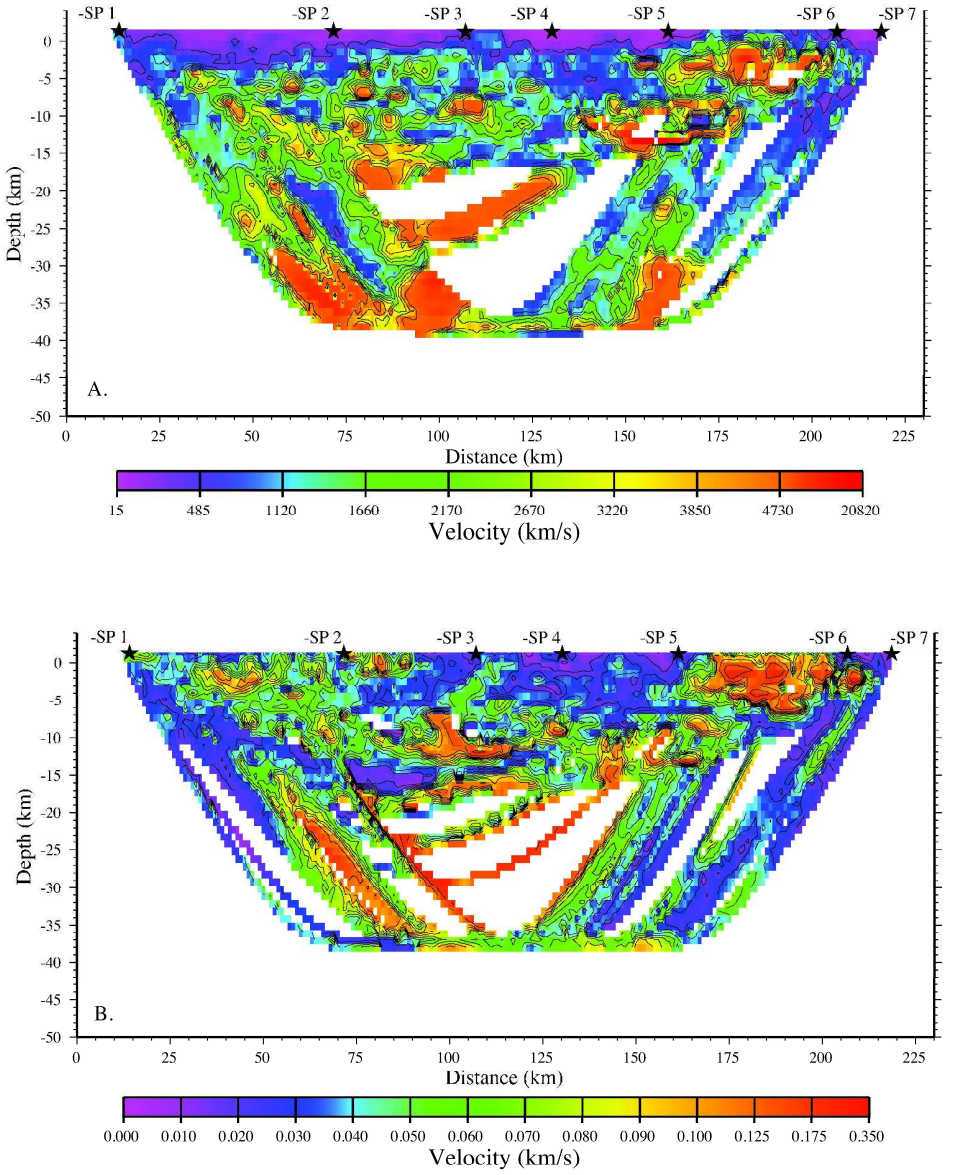

Figure 9 (Averill et al)

Fig. 9. Average RMS difference between the final velocity model and those produced through travel time sensitivity testing using Cauchy distributions to produce the random perturbations to the travel-time data. A. Average RMS difference produced using a Cauchy distribution for the perturbations. B. Average RMS difference produced with a modified Cauchy distribution. Perturbation values were limited to a 95% confidence interval.
194x245mm (600 x 600 DPI)